The Effect of Sample Holder Geometry on Electromagnetic Heating of Nanoparticle and NaCl Solutions at 13.56 MHz

Dongxiao Li, Yun Suk Jung, Hong Koo Kim, Junda Chen, David A. Geller, Mikhail V. Shuba, Sergey A. Maksimenko, Sarah Patch, Ebrahim Forati, and George W. Hanson*

***Abstract*—Electromagnetic absorption and subsequent heating of nanoparticle solutions and simple NaCl ionic solutions is examined for biomedical applications in the radiofrequency range at 13.56 MHz. It is shown via both theory and experiment that for *in vitro* measurements the shape of the solution container plays a major role in absorption and heating.**

***Index Terms*—Electromagnetic absorption, metal nanoparticles, nanoparticle solution.**

I. Introduction

NANOPARTICLE solutions are being investigated for thermal therapies and medical imaging technologies. In the former, applications to cancer treatments dominate, in which case electromagnetic energy is intended to cause localized heating of nanoparticles bound to cancer cells, or embedded in tumors, resulting in the selective destruction of the diseased tissue [1]–[3]. In the latter, such as photoacoustic and thermoacoustic imaging, electromagnetic energy is applied to a sample, generating heat, and subsequent thermal expansion, which produces an acoustic wave that is measured by an array of acoustic sensors [4], [5]. Differential heating in cancerous and noncancerous tissue, for example, can be used to produce an image, and the introduction of nanoparticles can provide contrast enhancement. Both areas of application are being investigated at near-infrared (NIR) and radiofrequencies (RF). The potential benefit of lower frequencies is the large penetration depth of electromagnetic energy in tissue, as well as the large volumes that can be interrogated. However, much less is known about electromagnetic heating of nanoparticle solutions at RF and other low frequencies compared to at NIR. In particular, nanoparticle absorption is very different at RF compared to NIR, where plasmonic effects are important. For *in vitro* experiments at low frequencies, the sample container (typically containing milliliter volumes) is immersed in the electromagnetic field, and container size and shape play an important role in subsequent heating. This is not the case at NIR, where all such macroscale samples are electrically large and usually a collimated beam is applied to a small area of the sample.

Absorption of RF energy by solutions of spherical nanoparticles has been of considerable recent interest [6]–[14]. However, for spherical nanoparticles, low-frequency absorption of energy is predicted to be very small, and it has recently been shown both experimentally and theoretically that spherical gold nanoparticles in colloidal solutions are themselves minimally heating at RF [15]–[18]. Heating is due to ionic content of the solutions, and the size and shape of the solution container is important in observing heating.

In this study, we focus on the effect of the shape of the solution container on RF electromagnetic heating, considering both nanoparticle solutions and simple saline (NaCl) ionic solutions. For *in vitro* measurements, the size and shape of the sample holder becomes very important, as does the impedance mismatch between the host medium and the sample. Assuming polarized electric fields, long thin cuvettes (e.g., test-tube like) can show absorption several orders of magnitude larger than spherical sample holders (e.g., the bottom of some glassware), which, in turn, can exhibit absorption that is much larger than thin disks typically used for cell cultures (e.g., Petri dishes). Measurements at RF (13.56 MHz) with various sample geometries containing gold nanoparticle or saline solutions clearly show this effect. We choose 13.56 MHz since this is in a low-frequency radio

Manuscript received May 19, 2012; revised September 5, 2012; accepted September 10, 2012. Date of publication September 14, 2012; date of current version November 22, 2012. This work was supported in part by the National Science Foundation (NSF)/Electrical, Communications and Cyber Systems Division (ECCS) (H.K.K), the Department of Health and Human Services (H.H.S.)/Health Resources and Services Administration (H.R.S.A), the Kanzius Cancer Research Foundation and the Pennsylvania Department of Community and Economic Development, the Paul Esposito Foundation for Liver & Bile Duct Cancer Research (D.A.G), and the National Institutes of Health (S.P. and E.F). The work of M.V. Shuba and S. A. Maksimenko was supported by the European Union (EU) under FP7 Grant FP7-230778 TERACAN and Grant FP7-266529 BY-NanoERA. *Asterisk indicates corresponding author.*

D. Li, Y. S. Jung, and H. K. Kim are with the Department of Electrical and Computer Engineering, Petersen Institute of NanoScience and Engineering, University of Pittsburgh, Pittsburgh, PA 15261 USA (e-mail: dongxli@gmail.com; yunjung.kor@gmail.com; kim@engr.pitt.edu).

J. Chen and D. A. Geller are with the Department of Surgery, Starzl Transplantation Institute, University of Pittsburgh, PA 15261 USA (e-mail: jundachen10@gmail.com; gellerda@upmc.edu).

M. V. Shuba and S. A. Maksimenko are with the Institute for Nuclear Problems, Belarus State University, 220030 Minsk, Belarus (e-mail: mikhail.shuba@gmail.com; sergey.maksimenko@gmail.com).

S. Patch is with the Department of Physics, University of Wisconsin-Milwaukee, Milwaukee, WI 53211 USA (e-mail: patchs@uwm.edu).

E. Forati is with the Department of Electrical Engineering, University of Wisconsin-Milwaukee, Milwaukee, WI 53211 USA (e-mail: eforati@uwm.edu).

*G. W. Hanson is with the Department of Electrical Engineering, University of Wisconsin-Milwaukee, Milwaukee, WI 53211 USA (e-mail: george@uwm.edu).

Color versions of one or more of the figures in this paper are available online at http://ieeexplore.ieee.org.

Digital Object Identifier 10.1109/TBME.2012.2219049

band reserved internationally for use in industrial, scientific, and medical purposes; the RF generator employed in this study operates at 13.56 MHz.

II. Permittivity of NaCl and Effective Permittivity of Nanoparticle Solutions

As a simple ionic solution, we consider NaCl, since its electrical properties are somewhat close to blood, and because of the importance of physiological saline in medical application. For saline, the Cole–Cole formula is used

$$\varepsilon_s(\omega) = \varepsilon_s(\infty) + \frac{\varepsilon_s(0) - \varepsilon_s(\infty)}{1 + (j\omega\tau)^{1-\alpha}} - j\frac{\sigma_s}{\omega\varepsilon_0} \tag{1}$$

where ω is angular frequency of the electromagnetic field, ε_0 is the vacuum permittivity, $\varepsilon_s(0) = 76$, $\varepsilon_s(\infty) = 4.5$, $\alpha \simeq 0.02$, $\sigma_s = 1.45$, and $\tau = 8.11$ ps for normal saline (see [19]–[21] and references therein). At 13.56 MHz, $\varepsilon_s = 76.0 - j1922.2$.

For nanoparticle solutions, we use the Maxwell–Garnett (MG) homogenized effective medium permittivity ε_{eff}. For low volume fractions of inclusions in a host medium, all such mixing formulas are equivalent [22]. Assuming spherical inclusions having isotropic relative permittivity ε_p in a host medium having isotropic relative permittivity ε_h, then [23]

$$\varepsilon_{\text{eff}} = \varepsilon_h \left(1 + \frac{3f_v \left(\frac{\varepsilon_p - \varepsilon_h}{\varepsilon_p + 2\varepsilon_h} \right)}{1 - f_v \left(\frac{\varepsilon_p - \varepsilon_h}{\varepsilon_p + 2\varepsilon_h} \right)} \right) \tag{2}$$

where $f_v = \rho_0 V$ is the volume fraction of spheres (ρ_0 is the number density of nanoparticles (m^{-3}) and $V = 4\pi a^3/3$ is the nanoparticle volume with a being the nanoparticle radius). Assuming typical gold values $\varepsilon_p \simeq 1 - j6.1 \times 10^{10}$, and $\varepsilon_h \simeq 80$ for water, such that for $f_v = 0.001$ we have $\varepsilon_{\text{eff}}/\varepsilon_h = 1.003 - j1.2 \times 10^{-11}$, and therefore, we can approximate the gold nanoparticle solution as having $\varepsilon_{\text{eff}} \simeq \varepsilon_h$. This is supported by recent experiment and theoretical work that showed that spherical gold nanoparticles in colloidal solutions are themselves minimally heating at RF [15]–[18]. Heating is due to ionic (impurity) content of the solutions [15], [18]; it has been shown that the conductivity of purified gold nanoparticle solutions was the same as DI water, justifying $\epsilon_{\text{eff}} \simeq \epsilon_h$.

Several comments on the validity of the MG effective permittivity are in order. First, the MG permittivity assumes low-volume fractions, such that mutual interactions among inclusions are negligible. Here, we consider $f_v \leq 10^{-3}$, and assume stable colloids. Second, the MG effective permittivity is independent of the actual size of the inclusions, and, as such, is an unrestricted theory in the sense that the resulting effective permittivity can be used in the same manner as any dielectric function [22]–[24]. In this study, this means that the effective permittivity can be used for the determination of electromagnetic absorption and subsequent solution heating. Extended effective medium formulations (typically formulated to account for higher multipole effects), which depend on the actual size of the inclusions, are restricted in their applicability, and generally cannot be used to compute absorption [22]–[24]. Third, the MG permittivity assumes that the inclusions are stationary. For nonspherical nanoparticles, one could consider a more general effective medium consisting of prolate spheroids which can rotate in an applied electric field via their permanent and/or induced dipole moment [25], resulting in an anisotropic and time-dependent medium. However, nanoscale objects exhibit a very low Reynolds number [26] and such rotations are too slow to respond to the applied field considered here. That is, negligible rotation can occur within a period of field oscillation for the frequencies of interest, since the period at the lowest considered frequency is $0.1\,\mu$s and typical rotation periods are on the order of milliseconds or longer [26]–[28]. Furthermore, even at much lower frequencies one would need a stronger electric field than typically encountered in thermal applications to overcome random thermal motion; potential energy of a dipole moment $\mathbf{p}$ in an electric field E is $W = -\mathbf{p}\cdot\mathbf{E}/2$, such that $|W_{\max}| = \alpha E^2/2$. With α on the order $10^{-30}\,\text{F}\cdot\text{m}^2$ as a typical value for long thin nanoparticles and electric fields on the order of 10^2–10^3 V/m inside the solution, then, assuming room temperature, $W/k_BT = 10^{-6}$–10^{-4}, where k_B is Boltzmann's constant and T is temperature. Thus, at the values of electric field typical of thermal applications, no dipole alignment can occur even if the frequency is sufficiently low. Similarly, any translational motion is negligible for the same reasons. Fourth, because the nanoparticles are immersed in an electrolytic solution, double layers can form at the nanoparticle-electrolyte interface [29], which can alter the dipole moment of the inclusions. However, processes establishing double layers are relatively slow, and double layer effects are most important below the megahertz range [29]. For gold nanoparticles in both deionized water and an ionic solution, it can be seen from Fig. 6 of [15] that double layer effects are unimportant above approximately 1 MHz. Thus, for the frequencies of interest here, the MG effective permittivity is an appropriate model.

III. Effect of Sample Holder Shape on Electromagnetic Energy Absorption and Heating Rates

The end goal of employing nanoparticles for thermal therapies or imaging is the generation of heat by the absorption of electromagnetic energy. Electromagnetic heating of simple solutions is also of importance in a variety of fields. The complex effective permittivity is an important aspect of heat generation, but the shape of the medium also plays an important role at RF. In all cases considered here, samples are small compared to wavelength, and so quasi-static conditions apply.

Upon application of an external electromagnetic field, for the initial period of absorption and heating, conduction and convection can be ignored and the heating rate (degrees/second) of a material sample is given by

$$\text{HR} = \frac{\partial T}{\partial t} = \frac{P}{\rho c_p V_s} \tag{3}$$

where T is temperature (K), t is time (s), P is the absorbed power (W), ρ is material mass density, V_s is the volume of the sample, and c_p is the material's specific heat (here, we use the density and specific heat of water, $\rho = 1000\,\text{kg/m}^3$ and $c_p =$

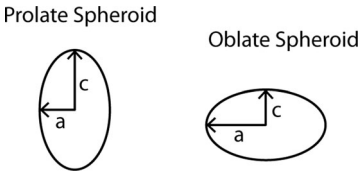

Fig. 1. Prolate and oblate spheroid geometries.

$4.18 \times 10^3\,\mathrm{J/kg \cdot K}$, although the specific heat will decrease somewhat for NaCl solutions compared with deionized water). The absorbed power is $P = \omega\varepsilon_0 \mathrm{Im}\left(-\varepsilon_s\right)|\mathbf{E}|^2 \mathrm{V_s}/2$ where ε_s is the relative permittivity of the sample, assuming a uniform electric field $\mathbf{E}$ throughout the sample (which occurs for general spheroids assuming quasi-static conditions). Then

$$\mathrm{HR} = \frac{\omega\varepsilon_0 \mathrm{Im}\left(-\varepsilon_s\right)|\mathbf{E}|^2}{2\rho c_p}. \tag{4}$$

When the electrical properties of the sample are different from that of the region surrounding the sample, the actual field inside the sample $\mathbf{E}$ is quite different from the applied (external) field. The interior field will depend both on electrical properties of the sample (permittivity) and sample geometry. In the following, we assume that a saline or saline-nanoparticle solution is contained in a spheroidal sample of given shape, and we ignore the effect of the sample holder material (i.e., the thin glassware containing the solution, which has very low absorption—the validity of this assumption was verified by the HFSS simulation discussed later).

For the sample holder, we assume a general spheroidal shape, with $a = b$ being the semiminor (prolate) and semimajor (oblate) axes, and c is the semimajor (prolate) and semiminor (oblate) axis of the sample, as depicted in Fig. 1.

Assuming an external electric field $\mathbf{E}^{\mathrm{ext}}$ polarized along an axis of the spheroid, the resulting quasi-static electric field inside the sample $\mathbf{E}^{\mathrm{int}}$ is [30]

$$\mathbf{E}^{\mathrm{int}} = \frac{1}{1 + N\left(\varepsilon_s/\varepsilon_{hs} - 1\right)}\mathbf{E}^{\mathrm{ext}} \tag{5}$$

where ε_{hs} is the relative permittivity of the material that serves as host of the sample (in the experiments described shortly, this medium is air), and N is the dimensionless depolarization factor along the direction of the electric field. The depolarization factors are

$$N_c = \frac{1 - e_p^2}{2e_p^3}\ln\left(\frac{1 + e_p}{1 - e_p} - 2e_p\right) \tag{6}$$

for a prolate spheroid ($a = b < c$), and

$$N_c = \frac{1 + e_o^2}{e_o^3}\left(e_o - \tan^{-1}\left(e_o\right)\right) \tag{7}$$

for an oblate spheroid ($a = b > c$), where $e_p = \sqrt{1 - a^2/c^2}$, $e_o = \sqrt{a^2/c^2 - 1}$, and $N_a = N_b = \left(1 - N_c\right)/2$.

Long thin samples (cuvette or test-tube-like) and flat disk (cell-culture-dish-like) samples are of obvious interest. For a prolate spheroid in the needle limit, $N_c \to 0$ and so $\mathbf{E}^{\mathrm{int}} \to \mathbf{E}^{\mathrm{ext}}$. For an oblate spheroid in the disk limit, $N_c \to 1$ and so

$$\mathbf{E}^{\mathrm{int}} = \frac{1}{1 + \left(\varepsilon_s/\varepsilon_{hs} - 1\right)}\mathbf{E}^{\mathrm{ext}} = \frac{\varepsilon_{hs}}{\varepsilon_s}\mathbf{E}^{\mathrm{ext}}. \tag{8}$$

Obviously, when $|\varepsilon_{hs}/\varepsilon_s| \ll 1$ such as occurs for nanoparticle and saline solutions in air, the interior field will be greatly reduced from the exterior field. This can also be thought of as an impedance mismatch issue, i.e., if $\varepsilon_s = \varepsilon_{hs}$ the interior field is the same as the exterior field for any geometry object. Disk-shaped objects such as used in cell cultures will exhibit considerably less heating than other sample geometries, and the maximum possible electric field will be found in long thin samples oriented parallel to the electric field.

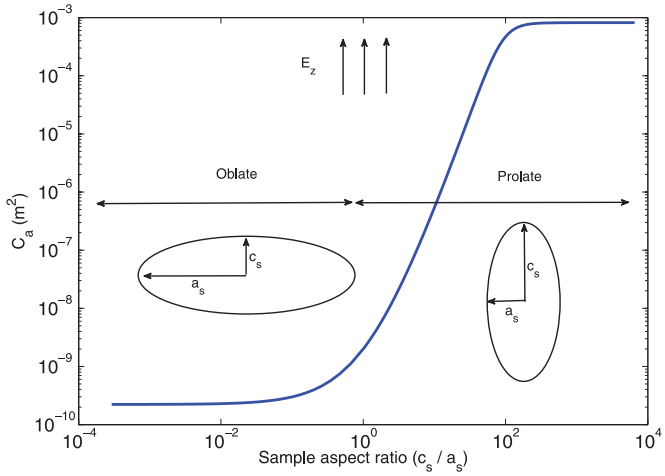

Fig. 2. Absorption cross section versus sample aspect ratio for a 1.5 mL saline spheroid at 13.56 MHz.

It is also instructive to consider the absorption cross section C_a (m^2) of the sample. Absorption cross section is absorbed power divided by incident (external) intensity ($I = |\mathbf{E}^{\mathrm{ext}}|^2/2\eta_{hs}$ $\mathrm{W/m}^2$, where $\eta_{hs} = \sqrt{\mu_{hs}/\varepsilon_{hs}}$ is the intrinsic impedance of the external medium) [31]. Fig. 2 shows the absorption cross section of a spheroid containing a normal saline medium as a function of sample aspect ratio $\mathrm{A} = c_s/a_s$ for a 1.5 mL saline filled spheroid immersed in air at 13.56 MHz. It is seen that in the extreme limits disk-like objects (with field parallel to the disk normal) have approximately seven orders of magnitude smaller absorption compared to needle-like objects.

IV. Effect of Sample Shape on Heating Rate: Comparison With Measurement

As discussed eralier, for *in vitro* measurements at RF frequencies the sample holder shape plays an important role in heating ([32]–[33] show a similar effect for whole-body absorption). To demonstrate this, we have performed measurements at 13.56 MHz on various sample holders containing normal saline and gold nanoparticle colloidal solutions (Ted Pella, #15711-20: 100-nm-diameter nanoparticles at 5.6×10^9 cm^{-3} concentration). Samples were placed between the transmission and reception heads of an RF generator (Therm Med LLC Kanzius machine; see Fig. 3) [34].

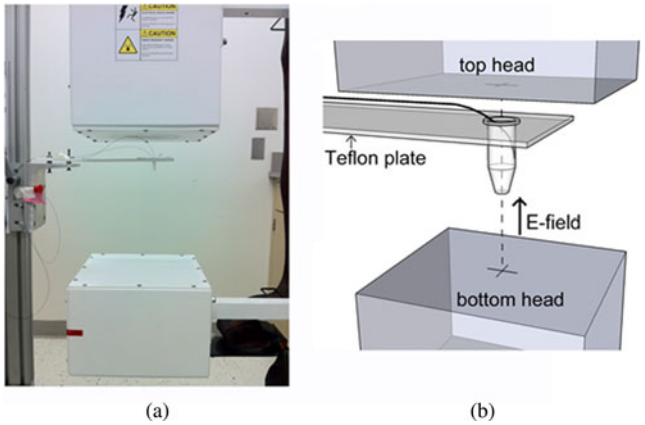

Fig. 3. Experimental setup for 13.56-MHz measurements.

Fig. 4. Container shapes containing solutions. Left to right: sphere (1 mL), tube (0.65 mL), prolate spheroid (0.7 mL), oblate spheroid (1 mL), dish (1 mL).

This generator consists of a power source coupled to the transmission/reception heads that are arranged in a coaxial end-fired configuration. The spacing between the transmission (top) and reception (bottom) heads was 30.5 cm, and a sample was placed at 5 cm below the top head. The E-field orients to the vertical direction. Note that the sample size is much smaller than the heads, and the E-field is expected to be reasonably uniform across the sample volume.

The temperature of the solutions was monitored with a fiber-optic temperature probe (LumaSense Technol. LUXTRON 812 Thermometer with STB Probe) immersed into the solution. Measurements were performed at a power level of 25 W, for which the electric field at the location of the sample is estimated to be 2.5 kV/m and approximately vertically oriented. The sample containers were made from quartz and are shown in Fig. 4. At 13.56 MHz, the permittivity of normal saline from (1) is approximately $76.0 - j1922$ ($\sigma \simeq 1.45$ S/m), and the measured permittivity of the nanoparticle stock solution was $100 - j55$ ($\sigma \simeq 0.04$ S/m). For the nanoparticle stock solutions, the large effective conductivity and the associated absorption are due to residual ions in the stock solution (i.e., due to the host medium of the nanoparticles ϵ_h, rather than due to the nanoparticles themselves) [15]; therefore, for the stock solution, we have $\epsilon_{\text{eff}} \simeq \epsilon_h = 100 - j55$.

Fig. 5 shows the measured temperature rise profiles of normal saline contained in the five different shaped sample holders. Fig. 6 shows the same thing for gold nanoparticle colloidal solutions. In all cases, the temperature probe was positioned in the

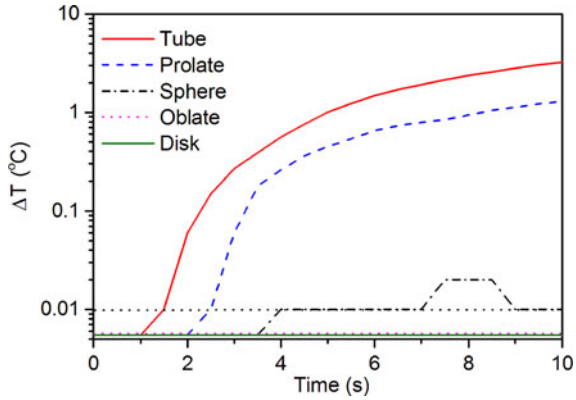

Fig. 5. Measured temperatures of normal saline contained in different spheroids at 13.56 MHz. The dotted line at $0.01°$C level indicates the resolution of temperature reading.

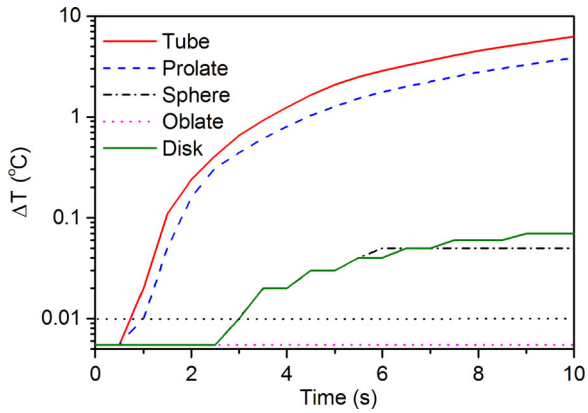

Fig. 6. Measured temperatures of 100-nm Au-NPs stock solution contained in different spheroids at 13.56 MHz. The dotted line at $0.01°$C level indicates the resolution of temperature reading.

middle of the sample. The volumes of the sample holders are noted in the caption of Fig. 4. The figures show a dramatic contrast (note the logarithmic scale) between the tube and prolate spheroid sample holders, which demonstrate a steep temperature rise, and the other sample shapes (sphere, oblate spheroid, and dish), which do not show any measurable increase for the same time interval. The gold nanoparticle solutions in the tube and prolate spheroid show slightly higher heating rates than for the saline case. This is due to different electrical conductivities of the background ionic solutions: 1.45 S/m for normal saline versus 0.04 S/m for gold nanoparticle solution [15]. The better absorption at $\sigma = 0.04$ S/m is consistent with theory as follows. For a given conductive medium spheroid, when conductivity is either zero or tending to infinity there will be no absorption. So, for some finite nonzero value of conductivity there will be maximum absorption. For a small prolate spheroid and a small sphere, equations for the value of conductivity that maximizes absorption are given by (30) and (37), respectively, in [35]. As an example, the value of conductivity that maximize absorption for a small 7-mm radius sphere (similar to that used here) with real-part permittivity 100 is $\sigma = 0.074$ S/m. Thus, the value of the conductivity of the nanoparticle stock solution is nearly optimal for a spherical sample, and absorption is expected to be

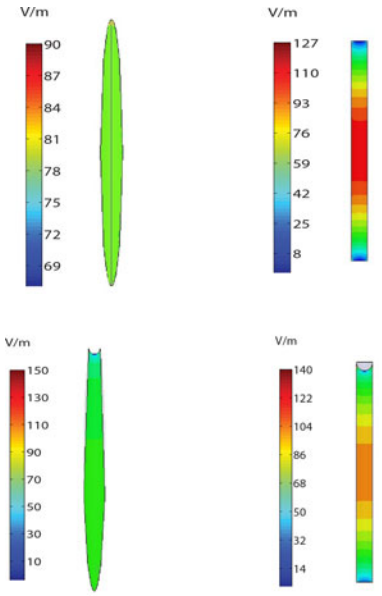

Fig. 7. Electric field distribution in the saline-filled prolate spheroid and tube sample holders (dimensions given in text) with (bottom row) and without (top row) a meniscus model. Applied field is 2.5 kV/m. For the cases without meniscus, in the prolate spheroid $|\mathbf{E}| = 81.88$, 81.81, and 81.81 V/m at the tube center (z= 0), 1/3 of the distance from the tube center (z = 9 mm), and 2/3 of the distance from the tube center (z= 18 mm), respectively, and for the tube, the corresponding values are $|\mathbf{E}| = 123.84$, 113.49, and 80.27 V/m. For the bottom row (with meniscus), the corresponding values are prolate spheroid: $|\mathbf{E}|$ =77.07, 74.54, and 66.39 V/m, tube:$|\mathbf{E}|$ =122.66, 112.11, and 79.10 V/m.

larger than when $\sigma = 1.45$ S/m. The conductivity dependence predicted in [35] was experimentally verified in [18] (see Fig. 9 therein).

For the simulation, the samples were modeled using the finite-element electromagnetic simulator HFSS (ANSYS Corporation) to obtain the total absorbed power and electric field distribution. For the prolate spheroid and tube sample holders, the HFSS-determined electric field distribution is shown in Fig. 7. The dimensions of the sample holders are roughly the same as in the measurements (prolate spheroid: major axis: 30 mm, minor axis: 2.5 mm, $N = 0.0153$; tube: radius = 2 mm, length = 53 mm). Regarding the top row, which shows the field in the absence of a meniscus, a few observations can be made concerning the field distributions: 1) the field in the prolate spheroid is uniform, consistent with quasi-static theory, 2) in the prolate spheroid the value of the field is $|\mathbf{E}| = 81.88$ V/m, also consistent with the prediction of (5) which gives $|\mathbf{E}| = 81.34$ V/m, 3) despite the prolate spheroid and tube having similar dimensions, the field in the tube is quite inhomogeneous, with $|\mathbf{E}| = 123.84$ V/m in the tube center, larger than the corresponding value in the prolate spheroid.

The bottom row of Fig. 7 shows the effect of the presence of a meniscus using a crude nonself-consistent hemispherical model of meniscus (the top hemispherical region is air and the remainder of the tube is filled with normal saline). The presence of a meniscus considerably alters the field in the vicinity of the meniscus, but has a moderately small effect on field values elsewhere in the sample. It can be seen that much higher electric fields are found in the meniscus region, as shown in the closeup

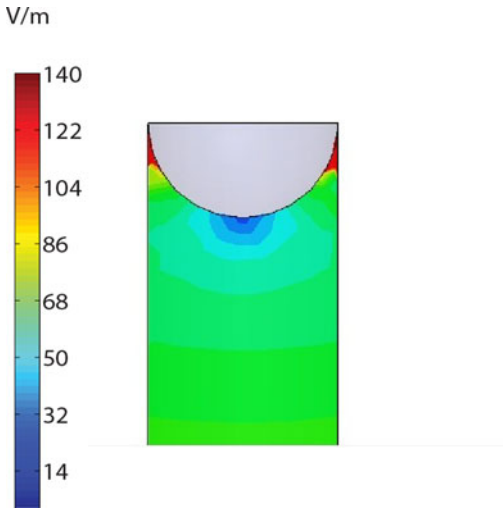

Fig. 8. Electric field distribution in the vicinity of a meniscus model. Applied field is 2.5 kV/m.

TABLE I
COMPARISON OF SIMULATED [COMPUTED USING HFSS AND (9) AND (10)] AND MEASURED HEATING RATE (DEGREES/S) FOR NORMAL SALINE AT 13.56 MHZ

	HR (°C/s) HFSS, (9)	HR (°C/s) HFSS, (10)	HR (°C/s) Measurement
Tube	0.0018	0.0027	0.02
Prolate	0.0011	0.0012	<0.01
Sphere	3.34×10^{-6}	3.10×10^{-6}	<0.001
Oblate	0.63×10^{-6}	0.54×10^{-6}	<0.001
Dish	1.63×10^{-6}	0.33×10^{-6}	<0.001

TABLE II
COMPARISON OF SIMULATED [COMPUTED USING HFSS AND (9) AND (10)] AND MEASURED HEATING RATE (DEGREES/S) FOR GOLD NANOPARTICLE STOCK SOLUTION AT 13.56 MHZ

	HR (°C/s) HFSS, (9)	HR (°C/s) HFSS, (10)	HR (°C/s) Measurement
Tube	0.0048	0.0078	0.02
Prolate	0.0034	0.0037	0.01
Sphere	20.0×10^{-6}	21.0×10^{-6}	<0.001
Oblate	4.40×10^{-6}	4.30×10^{-6}	<0.001
Dish	6.10×10^{-6}	2.74×10^{-6}	<0.001

Fig. 8 for the tube case, consistent with our experimental observations that sometimes sparking occurs in this region (when RF power greater than 100 W was applied).

The adiabatic heating rate was then calculated (appropriate to the early time of heating, before conduction and convection become important), based on total absorbed power

$$\mathrm{HR_G} = \frac{P}{\rho c_p V_s} \tag{9}$$

where P is absorbed power in W. As described previously, for ρ and c_p, we assume values for water. One could also define a local adiabatic heating rate based on the electric field at a point

$$\mathrm{HR_L}(\mathbf{r}) = \frac{\frac{1}{2}\sigma\,|\mathbf{E}(\mathbf{r})|^2}{\rho c_p}. \tag{10}$$

The experimental temperature probe locations was near the middle of the sample. The measured and simulated heating rates are summarized in Tables I and II. The measured heating rates

were determined over the first 1–2 s of heating for the tube and prolate samples (which heated quickly), and 100 s for the sphere, oblate, and dish samples (which did not heat appreciably even for long time periods). The resolution of temperature reading is 0.01°C, and therefore, the resolution of heating rate reading is estimated be 0.01°C/s for a time span of 1 s, or 0.001°C/s for a 10-s span. For the sphere, dish, and oblate spheroid cases the measured rate is an upper bound, and accurate measurements are not available due to the minimal heating involved.

The tables confirm the general trend predicted by HFSS and quasi-static theory based on (5), showing the importance of sample container shape on heating rate. Thus, in drawing conclusions on the heating ability of a solution, it is important to use an appropriately shaped container (e.g., Petri-type dishes in a vertically aligned field will show little or no heating, even though the substance itself may be a very good RF absorber). This is a particular aspect of lower frequency work, as opposed to typical NIR measurement where the wavelength is significantly smaller than the container size. The lower heating rates for the sphere, oblate, and dish geometries are due to the fact that the interior electric field (5) is much lower than for the tube or prolate spheroid case. We attribute the difference between measurement and simulation to be due primarily to uncertainty in the actual value of electric field applied to the sample (heating rate depending on the square of this field value), and to a possible variation of the applied field over the sample volume. It should be noted that we only report the heating rate at the very early stages of heating. Convection and conduction effects quickly lead to a nonlinear response, as evidenced in Figs. 5 and 6. These effects will play an important role in overall heating, but need to be considered by more sophisticated models (especially convection), which is beyond the scope of this study.

One purpose of this study is to demonstrate that at lower frequencies the shape of the container holding a nanoparticle solution (or any conductive solution) for *in vitro* measurements plays an important role, and subsequent heating must be considered in the light of container shape. However, this also points to similar effects for small animal whole-body studies. For example, a long, thin subject immersed in an RF field and oriented parallel to the field will allow a larger electric field to penetrate into the interior compared to a more spherical subject. Body shape must be properly accounted for in the interpretation of subsequent heating results.

V. Conclusion

Electromagnetic absorption and heating of nanoparticle solutions has been examined at 13.56 MHz. It has been shown by theory and experiment that for linearly polarized electric fields it is important to take into account container shape and orientation when measuring electromagnetic heating of samples at RF.

Acknowledgment

The authors would like to thank Á. Delgado, Departamento de Física Aplicada, Facultad de Ciencias, Campus Fuentenueva, Universidad de Granada, Granada, Spain, for helpful discussions concerning double-layer effects.

References

[1] C. Vauthier, N. Tsapis, and P. Couvreur, "Nanoparticles: Heating tumors to death," *Future Medic.*, vol. 6, pp. 99–109, Jan. 2011.

[2] L. C. Kennedy, L. R. Bickford, N. A. Lewinski, A. J. Coughlin, Y. Hu, E. S. Day, J. L. West, and R. A. Drezek, "A new era for cancer treatment: Gold-nanoparticle mediated thermal therapies," *Small*, vol. 7, pp. 169–83, Jan. 2011.

[3] X. Huang, P. K. Jain, I. H. El-Sayed, and M. A. El-Sayed, "Plasmonic photothermal therapy (PPTT) using gold nanoparticles," *Lasers Med. Sci.*, vol. 23, pp. 217–228, 2008.

[4] M. Pramanik, M. Swierczewska, D. Green, B. Sitharaman, and L. V. Wang, "Single-walled carbon nanotubes as a multimodal-thermoacoustic and photoacoustic-contrast agent," *J. Biomed. Opt.*, vol. 14, p. 034018(1–8), Jan. 2009.

[5] A. de la Zerda, C. Zavaleta, S. Keren, S. Vaithilingam, S. Bodapati, Z. Liu, J. Levi, B. R. Smith, T. J. Ma, O. Oralkan, Z. Cheng, X. Chen, H. Dai, B. T. Khuri-Yakub, and S. S. Gambhi, "Carbon nanotubes as photoacoustic molecular imaging agents in living mice," *Nature Nanotechnol.*, vol. 3, pp. 557–562, Sep. 2008.

[6] S. A. Curley, P. Cherukuri, K. Briggs, C. R. Patra, M. Upton, E. Dolson, and P. Mukherjee, "Noninvasive radiofrequency field-induced hyperthermic cytotoxicity in human cancer cells using cetuximab-targeted gold nanoparticles," *J. Exper. Therap. Oncol.*, vol. 7, pp. 313–326, 2008.

[7] C. J. Gannon, C. R. Patra, R. Bhattacharya, P. Mukherjee, and S. A. Curley, "Intracellular gold nanoparticles enhance non-invasive radiofrequency thermal destruction of human gastrointestinal cancer cells," *J. Nanobiotechnol.*, vol. 6, p. 2(1–9), Jan. 2008. doi:10.1186/1477-3155-6-2. Available: http://www.jnanobiotechnology.com/content/pdf/1477-3155-6-2.pdf

[8] J. Cardinal, J. Klune, E. Chory, G. Jeyabalan, J. Kanzius, M. Nalesnik, and D. Geller, "Non-invasive radiofrequency ablation of cancer targeted by gold nanoparticles," *Surgery*, vol. 144, pp. 125–132, Aug. 2008.

[9] C. H. Moran, S. M. Wainerdi, T. K. Cherukuri, C. Kittrell, B. J. Wiley, N. W. Nicholas, S. A. Curley, J. S. Kanzius, and P. C. Cherukuri, "Size dependent joule heating of gold nanoparticles using capacitively coupled radiofrequency fields," *Nano Res.*, vol. 2, pp. 400–405, 2009.

[10] P. Cherukuri, E. S. Glazera, and S. A. Curley, "Targeted hyperthermia using metal nanoparticles," *Adv. Drug Del. Rev.*, vol. 62, pp. 339–345, 2010.

[11] P. Cherukuri and S. A. Curley, "Use of nanoparticles for targeted, noninvasive thermal destruction of malignant cells," *Cancer Nanotechnol. Meth. Molecul. Biol.*, vol. 624, pp. 359–373, 2010.

[12] E. S. Glazer, K. L. Massey, C. Zhu, and S. A. Curley, "Pancreatic carcinoma cells are susceptible to noninvasive radio frequency fields after treatment with targeted gold nanoparticles," *Surgery*, vol. 148, pp. 319–324, Aug. 2010.

[13] E. S. Glazer, C. Zhu, K. L. Massey, C. S. Thompson, W. D. Kaluarachchi, A. N. Hamir, and S. A. Curley, "Noninvasive radiofrequency field destruction of pancreatic adenocarcinoma xenografts treated with targeted gold nanoparticles," *Clin. Cancer Res.*, vol. 16, pp. 5712–5721, 2010.

[14] D. E. Kruse, D. N. Stephens, H. A. Lindfors, E. S. Ingham, E. E. Paoli, and K. W. Ferrara, "A radio-frequency coupling network for heating of citrate-coated gold nanoparticles for cancer therapy: Design and analysis," *IEEE Trans. Biomed. Eng.*, vol. 58, no. 7, pp. 2002–2012, Jul. 2011.

[15] D. Li, Y. S. Jung, S. Tan, H. K. Kim, E. Chory, and D. A. Geller, "Negligible absorption of radiofrequency radiation by colloidal gold nanoparticles," *J. Colloid Interface Sci.*, vol. 358, pp. 47–53, Jan. 2011.

[16] G. W. Hanson, R.C. Montreal, and S. P. Apell, "Electromagnetic absorption mechanisms in metal nanospheres: Bulk and surface effects in radiofrequency-terahertz heating of nanoparticles," *J. Appl. Phys.*, vol. 109, pp. 124306-1–124306-6, 2011.

[17] E. Sassaroli, K. C. P. Li, and B. E O'Neill, "Radio frequency absorption in gold nanoparticle suspensions: A phenomenological study," *J. Phys. D*, vol. 45, pp. 075303-1–075303-15, 2012.

[18] X. Liu, H.-J. Chen, X. Chen, C. Parini, and D. Wen, "Low frequency heating of gold nanoparticle dispersions for non-invasive thermal therapies," *Nanoscale*, vol. 4, pp. 3945–3953, 2012.

[19] C. Gabriel and A. Peyman, "Dielectric measurement: Error analysis and assessment of uncertainty," *Phys. Med. Biol.*, vol. 51, pp. 6033–6046, 2006.

[20] A. Nyshadham, C. L. Sibbald, and S. S. Stuchly, "Permittivity measurements using open-ended sensors and reference liquid calibration-an uncertainty analysis," *IEEE Trans. Microw. Theory Techs.*, vol. 40, no. 2, pp. 305–314, Feb. 1992.
[21] H. M. Gach and T. Nair, "Radiofrequency interaction with conductive colloids: Permittivity and electrical conductivity of single-wall carbon nanotubes in saline," *Bioelectromagnetics*, vol. 31, pp. 582–588, 2010.
[22] C. F. Bohren, "Applicability of effective-medium theories to problems of scattering and absorption by nonhomogeneous atmospheric particles," *J. Atmosph. Sci.*, vol. 43, pp. 468–475, Mar. 1986.
[23] A. Sihvola, *Electromagnetic Mixing Formulas and Applications*. London: IEE press, 1999.
[24] R. Ruppin, "Evaluation of extended Maxwell-Garnet theories," *Opt. Commun.*, vol. 184, pp. 273–279, Aug. 2000.
[25] T. B. Jones, *Electromechanics of Particles*. Cambridge, U.K.: Cambridge Univ. Press, 2005.
[26] D. L. Fan, F. Q. Zhu, R. C. Cammarata, and C. L. Chien, "Controllable high-speed rotation of nanowires," *Phys. Rev. Letts.*, vol. 94, pp. 247208-1–247208-4, Jun. 2005.
[27] T. J. Robb-Smith, K. J. Donovan, K. Scott, and M. Somerto, "Induced electro-optic effects in single-walled carbon nanotubes. II. Hydrodynamics of nanotubes in viscous media," *Phys. Rev. B*, vol. 83, pp. 155415-1–155415-7, Apr. 2011.
[28] F. M. Zimmermann and J. W. Shan, "Rotational friction of single-wall carbon nanotubes in liquid suspension," *Appl. Phys. Letts.*, vol. 94, pp. 053107-1–053107-3, Feb. 2009.
[29] C. Grosse and A. V. Delgado, "Dielectric dispersion in aqueous colloidal systems," *Curr. Opin. Colloid Interf. Sci.*, vol. 15, pp. 145–159, Jun. 2010.
[30] A. M. Portis, *Electromagnetic Fields: Sources and Media*. New York: Wiley, 1978.
[31] C. F. Bohren and D. R. Huffman, *Absorption and Scattering of Light by Small Particles*. New York: Wiley, 1983.
[32] O. P. Gandhi, "Frequency and orientation effects on whole animal absorption of electromagnetic waves," *IEEE Trans. Biomed. Eng.*, vol. BME-22, no. 6, pp. 536–542, Nov. 1975.
[33] H. Massoudi, C. H. Durney, and C. C. Johnson, "Long-wavelength electromagnetic power absorption in ellipsoidal model of man and animals," *IEEE Trans. Microw. Theory Tech.*, vol. 25, no. 1, pp. 47–52, Jan. 1977.
[34] J. S. Kanzius, U.S. Patent Publication Nos. US 2006/0 190 063 A1, US 2005/ 0 2511 233 A1, US 2005/0 251 234 A1, and World Intellectual Property Organization WO 2007/027 614.
[35] G. W. Hanson and S. K. Patch, "Optimum electromagnetic heating of nanoparticle thermal contrast agents at RF frequencies," *J. Appl. Phys.*, vol. 106, pp. 054309-1–054309-10, Sep. 2009.

Authors' photographs and biographies not available at the time of publication.